Influence of $k_\perp$ broadening on ARPES spectra of the (110) and (001) surfaces of $SrVO_3$ films

T. Mitsuhashi,[1,2] M. Minohara,[2] R. Yukawa,[2] M. Kitamura,[2] K. Horiba,[2] M. Kobayashi,[2,*] and H. Kumigashira[1,2]

[1]*Department of Physics, Tohoku University, Sendai 980-8578, Japan*

[2]*Photon Factory, Institute of Materials Structure Science, High Energy Accelerator Research Organization (KEK), 1-1 Oho, Tsukuba 305-0801, Japan*

(Received 25 July 2016; revised manuscript received 31 August 2016; published 28 September 2016)

To examine the effect of $k_\perp$ broadening on angle-resolved photoemission spectroscopy (ARPES) spectra, *in situ* ARPES using the variable polarization of synchrotron light has been performed for the (110) and (001) surfaces of $SrVO_3$ films. Using the polarization dependence for the band structures of the V $3d$ t_{2g} states, we have separately observed the d_{xy}-derived states and the d_{yz}/d_{zx} ones for the (110) surface. It is found that ARPES images for the d_{yz}/d_{zx} states are considerably broader than those for the d_{xy} states. Meanwhile, such a broadening is not observed in the identical d_{yz}/d_{zx}-derived band dispersion along the crystallographically equivalent direction on the (001) surface, indicating that the broadening of the ARPES image originates from the absence or presence of mirror symmetry in the respective states with respect to the ARPES-measurement planes. The observed spectroscopic behavior is well reproduced by the simulation where the $k_\perp$ broadening in the photoelectron emission process is taken into account. These results indicate that the consideration of the mirror symmetry of the band structures with respect to the ARPES-measurement plane is important for analyzing the ARPES-spectral line shape in the case that the $k_\perp$-broadening effect is dominant in ARPES spectra.

DOI: 10.1103/PhysRevB.94.125148

I. INTRODUCTION

The "$k_\perp$ broadening" is a fundamental phenomenon in the photoelectron emission process from a solid: Owing to the short escape depth of photoelectrons (Δz), significant broadening of the momentum perpendicular to the surface ($\Delta k_\perp$) occurs due to the uncertainty principle ($\Delta z\, \Delta k_\perp \sim 1$) [1–3]. As a result of $k_\perp$ broadening, the line shape of an angle-resolved photoemission spectroscopy (ARPES) spectrum from the corresponding $\boldsymbol{k}$ point, which is determined by the function of photon energy ($h\nu$) and emission angle (θ) normal to the surface [4], is strongly influenced by whether or not the point with zero group velocity (v_g) along the $k_\perp$ direction ($v_g = \partial E/\partial k_\perp = 0$) exists in the vicinity of the measured $\boldsymbol{k}$ point. This is because the density of states (DOS) is considerably larger at this van Hove singularity (vHS) point.

The effect of $k_\perp$ broadening becomes prominent for ARPES spectra measured at surface-sensitive photon energies. In the case of the ARPES using vacuum ultraviolet (VUV) light, the value of $\Delta k_\perp$ (Δz) is typically in the range of 0.25–1 $Å^{-1}$ (1–4 Å) [5,6]. Therefore, the $k_\perp$ broadening considerably affects the line shape of the VUV-ARPES spectra for three-dimensional (3D) materials [2,7–10]. In particular, it is expected that the $k_\perp$-broadening effect strongly depends on the existence of mirror symmetry in the observed states with respect to the ARPES-measured high-symmetry line (plane) because the vHS point always exists on the high-symmetry line (plane) in this case. Thus, it is crucial to investigate how the ARPES spectra change depending on the presence or absence of vHS at the measurement line (plane). However, irrespective of its importance to ARPES analysis, there are few investigations for identifying the influence of the $k_\perp$ broadening on ARPES spectra of 3D materials [2,11,12].

In this study, we have employed the (110) and (001) surfaces of $SrVO_3$ (SVO) films for the investigation. SVO is a typical Fermi-liquid metal with the simple $3d^1$ configuration, and its electronic structures can be essentially considered to consist of three orthogonal t_{2g} orbitals of V $3d$ states [13,14]. The band structures of V $3d$ states located near the Fermi level (E_F) is well described by the renormalization scheme of the tight-binding (TB) calculations [15,16]. According to the band-structure calculation, the Fermi-surface (FS) sheets of bulk SVO with cubic symmetry (Fig. 1) are essentially formed from three intersecting cylinders containing the V-$3d$ d_{xy}, d_{yz}, and d_{zx} states [14,16–18]. Each state has a two-dimensional (2D) character in the respective xy (110), yz (011), and zx (101) planes. By considering the existence of mirror symmetry with respect to the ARPES-measured plane (yellow hatched plate in Fig. 1), it is expected for the (110) surface that the d_{xy}-derived state has a large DOS at the ΓMRX measured plane, whereas d_{yz}/d_{zx} states do not, owing to the absence of vHS apart from the Γ point. In contrast, for the (001) surface, all three orbital derived states have vHS at the ΓMX plane where ARPES are measured. Therefore, the two surfaces are good examples for investigating the influence of $k_\perp$ broadening on the ARPES spectra and its mirror-symmetry dependence.

Wang *et al.* recently performed an ARPES study on the metallic Ti $3d$ t_{2g} states appearing at the (110) surface of doped $SrTiO_3$ (STO) and reported significantly different behaviors between d_{xy}-derived states and d_{yz}/d_{zx} states [19]. Although it is difficult to directly compare these data on (110) with other previously reported ARPES results on the STO (001) surface owing to the differences in the experimental conditions, the observed behavior of d_{yz}/d_{zx} states at the (110) surfaces [19,20] seems to be quite different from the (001) case [21–30]. Thus, the systematic studies of the influence of $k_\perp$ broadening on the ARPES spectra is also important for understating the behavior of the two-dimensional electron-gas (2DEG) states appearing at the surfaces of STO [20,31] and $KTaO_3$ [32–34] as well as at the interface of $LaAlO_3/SrTiO_3$ [35,36].

*Author to whom correspondence should be addressed: masakik@post.kek.jp

 ©2016 American Physical Society

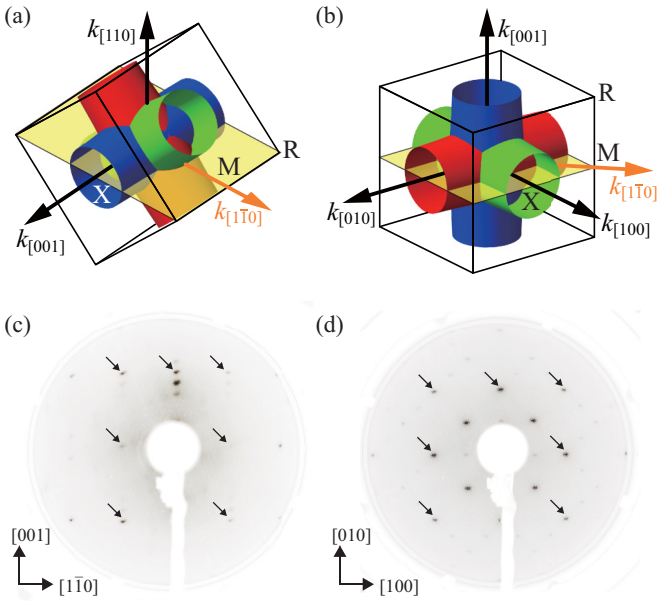

FIG. 1. Schematic of the FSs of $SrVO_3$ at (a) the (110) surface and (b) the (001) surface. Cylindrical FSs of the d_{xy} (blue), d_{yz} (green), and d_{zx} (red) orbitals cross each other at the Γ point. The yellow plates in (a) and (b) represent the Γ*MRX* and Γ*MX* planes where the ARPES spectra are measured (ARPES-measured planes). The orange arrow indicates the crystallographically equivalent Γ-*M* direction. (c) LEED pattern obtained at the (110) surface of the $SrVO_3$ films. The sharp 1×1 spots with surface-reconstruction-derived 1×6 spots are clearly observed. (d) LEED pattern obtained at the (001) surface. The sharp 1×1 spots are also observed in addition to the surface-reconstruction-derived $c(2 \times 2)$ spots.

In this paper, we report the results of *in situ* polarization-dependent ARPES measurements of the SVO films grown on the (110)- and (001)-oriented STO substrates, along with a detailed ARPES-spectra simulation considering the $k_\perp$-broadening effect. On the (110) surface of SVO, the ARPES images for the d_{yz}/d_{zx} states are considerably broader than those for the d_{xy} states. In contrast, such broadening was not observed in the d_{yz}/d_{zx}-derived band dispersion along the crystallographically equivalent direction on the (001) surface, indicating that the broadening of the ARPES image originates from the absence or presence of mirror symmetry in the corresponding states with respect to the ARPES-measured planes. The spectroscopic behavior is well reproduced by the ARPES-spectra simulation where the $k_\perp$ broadening in the photoelectron emission process is accordingly incorporated. These results indicate that the consideration of the mirror symmetry of band structures with respect to the ARPES-measured plane is important for analyzing the ARPES-spectral line shape in the case that the $k_\perp$-broadening effect is dominant in ARPES spectra.

II. EXPERIMENTAL

Experiments were carried out using a photoemission spectroscopy system combined with a laser molecular-beam epitaxy chamber [37], which was installed at the beamline BL-2A MUSASHI of Photon Factory, KEK. SVO films with a thickness of 100 monolayers were grown onto (110)- and (001)-oriented 0.05 wt % Nb-doped STO substrates by pulsed laser deposition. During deposition, the substrate temperature was kept at 750 °C for SVO (110) films and 900 °C for (001) ones under an ultrahigh vacuum of 10^{-8} Torr. During the growth, the intensity of the specular spot in the reflection high-energy electron-diffraction (RHEED) pattern was monitored to determine the surface morphology and the film growth rate. The epitaxial growth of the SVO thin films on the STO substrates for both the orientations was confirmed by the observation of clear RHEED oscillations due to the layer-by-layer growth mode. After cooling to below 100 °C, the films were moved into the photoemission chamber under an ultrahigh vacuum of 10^{-10} Torr. The in-vacuum transfer was necessary to maintain the highest-quality surface.

The ARPES experiments were conducted *in situ* at 20 K using two orthogonally linear polarizations from the incident light with $h\nu = 36$–94 eV in the VUV region while using linear-horizontal (LH) incident light with $h\nu = 440$–560 eV in the soft-x-ray (SX) region, see the Supplemental Material [38]. The energy resolutions were set to be approximately 15–20 meV for VUV-ARPES measurements and 200–250 meV for SX ones, while angular resolutions were set to be about 0.2°. E_F of the samples was referred to that of a gold foil that was in electrical contact with the sample. Detailed ARPES-measurement conditions are described elsewhere [16], see the Supplemental Material [38]. The surface structure and cleanness of the vacuum-transferred SVO films were checked by low-energy electron-diffraction (LEED) and core-level photoemission measurements. As shown in Figs. 1(c) and 1(d), the sharp 1×1 spots with surface reconstruction-derived spots were observed for both the (110) and (001) surfaces of SVO films, confirming their well-ordered surfaces. No detectable C 1*s* peak was observed in the core-level photoemission spectra. These results indicate that no cleaning procedure was needed for the *in situ* ARPES measurements. The surface morphology of the measured SVO thin films was analyzed by *ex situ* atomic force microscopy in the air, and atomically flat step-and-terrace structures were observed. The crystal structure was characterized by four-circle x-ray diffraction, confirming the coherent growth of SVO films onto Nb:STO substrates for both the orientations.

III. RESULTS AND DISCUSSION

A. *In situ* polarization-dependent ARPES spectra

Figure 2 shows the result of out-of-plane FS mapping for the SVO (110) film obtained from *in situ* normal-emission ARPES measurements for the Γ*MX* emission plane (the blue hatched area) in the Brillouin zone (BZ) shown in Figs. 2(a) and 2(b). Figures 2(c) and 2(d) show the FS mappings, which are measured by varying the photon energies from 36 to 94 eV, taken with the LH and linear-vertical (LV) polarizations of incident light, respectively, see the Supplemental Material [38]. Significant polarization dependence is clearly observed. By taking the present experimental geometry into account, ARPES intensities of d_{xy}- (d_{yz}/d_{zx}-) derived bands become dominant in the LH (LV) mode, whereas those of the d_{yz}/d_{zx}- (d_{xy}-) derived states are considerably suppressed

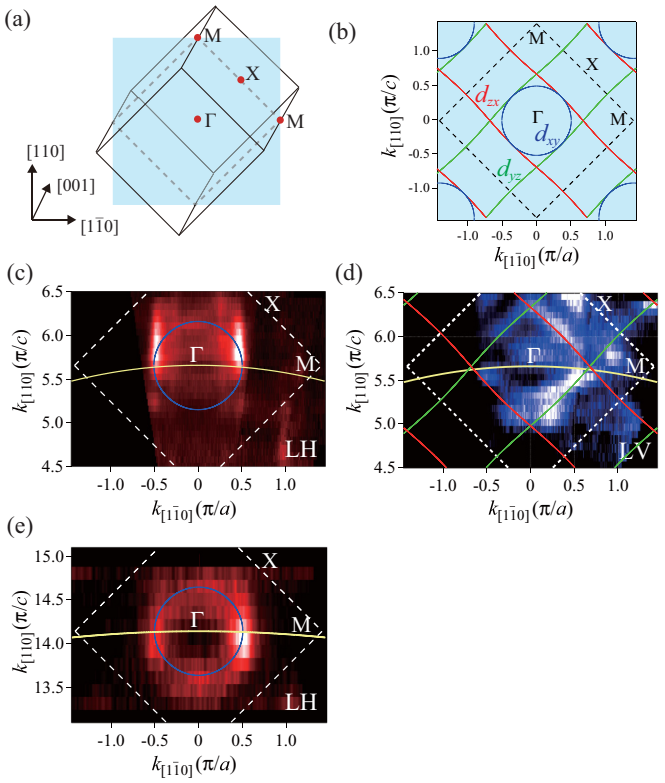

FIG. 2. Out-of-plane FSs of $SrVO_3$ (110) films determined from the normal-emission ARPES measurements. (a) BZ of the SVO (110) surface. Normal-emission ARPES measurements were performed for the ΓMX emission plane (hatched by blue). (b) FSs calculated from the TB calculation for the ARPES emission (the ΓMX) plane. The blue circle FS centered at the Γ point originates from the d_{xy} states, while the parallel green and red lines originate from the d_{yz} and d_{zx} ones. (c) Out-of-plane FS mapping taken at the photon energies from 36 to 94 eV using LH light. The FS calculated for the d_{xy} states is superimposed. The yellow thick line is the trajectory of the measured $\boldsymbol{k}$ point of the ARPES measurement at 66 eV calculated using Eq. (2) with the inner potential of 20 eV. (d) Out-of-plane FS mapping using LV where the FSs calculated for the d_{yz} and d_{zx} states are superimposed. (e) FS mapping taken at the bulk-sensitive photon energies from 440 to 560 eV with LH light, together with the results of the TB calculation for the d_{xy} states. It should be noted that ARPES intensities of d_{xy}- (d_{yz}/d_{zx}-) derived bands become dominant in the LH (LV) mode, owing to the dipole selection rules for these light polarizations and measurement geometries used [38].

owing to the dipole selection rules [39]. In other words, the polarization-dependent ARPES enables the determination of the FSs of d_{xy} states and d_{yz}/d_{zx} states separately. In comparison with the results of TB calculation [14], the overall shape of the FS seems to be in good agreement between the experiments and the calculations for d_{yz}/d_{zx}-derived states. However, as shown in Fig. 2(c), there are significant differences between the observation and the calculation for d_{xy} states: The FS shape of d_{xy} states around the Γ-M high-symmetry line is considerably elongated along the $k_\perp$ direction, whereas such an effect is hardly seen in d_{yz}/d_{zx}-derived states. Such elongation has also been reported in previous ARPES results on 3D materials [40–43]. By considering the mirror symmetry of each state with respect to the measured Γ-M high-symmetry line [see Figs. 1(a) and 1(b)], it is suggested that the observed elongation may originate from the $k_\perp$ broadening, see the Supplemental Material [38]. Indeed, the elongation behavior along the $k_\perp$ direction is considerably suppressed in the FS mapping in the same region of the BZ obtained by SX photons (440–560 eV) as shown in Fig. 2(e), reflecting the relatively longer escape depth of the photoelectron in this energy region (5–11 Å) than that in the VUV region (1–4 Å) [6].

To elucidate the influence of $k_\perp$ broadening on the ARPES spectra, we have performed polarization-dependent ARPES measurements along the Γ-M direction on the (110) surface [Fig. 1(a)] as well as the in-plane FS mappings of the ARPES-measured ΓMRX plane shown in Figs. 3(a) and 3(b) (k_x-k_y planes with $k_\perp = n\pi/a$, where a is the lattice constant of SVO; $n = 2$ in the present case). The results are shown in Figs. 3(c)–3(h), together with corresponding TB calculations in the renormalization scheme with a renormalization factor of $Z = 0.5$. It should be noted that we set the color-scale level in Figs. 3(e) and 3(f) so that the apparent width of momentum distribution curves (MDCs) in the color-scale image is almost equal to the half width at half maximum of the MDC of the corresponding band. There are significant differences in the FS mappings and ARPES images taken with LH and LV polarizations: Owing to the dipole selection rules for these light polarizations and measurement geometries used, see the Supplemental Material [38] and Ref. [39], only the d_{xy}-derived states are best observed along the Γ-M direction with the LH polarization, whereas the d_{yz}/d_{zx}-derived states are best observed with LV. This assignment is further confirmed by the comparison with the TB calculations.

Regarding the width of the MDC in the parabolic band dispersion in Figs. 3(e) and 3(f), we immediately notice that the MDC width of the observed d_{yz}/d_{zx} bands is much broader than that of the d_{xy} band. The width of the MDC for the d_{yz}/d_{zx} bands is evaluated to be $0.52\pi/a$, while that for the d_{xy} band is $0.13\pi/a$. In general, the inverse lifetime ($\hbar/\tau$) and Fermi velocity (v_F) of electrons and the angular resolution in the spectrometer are mainly contributed to the width of the MDC. In the present case: (i) The inverse lifetime, which mainly reflects the self-energy of an electron in the SVO, is expected to have almost the same values for each t_{2g} orbital, (ii) the difference in the Fermi velocity of the d_{xy} and d_{yz}/d_{zx} bands along the Γ-M direction is estimated to be 2.3×10^5 and 3.3×10^5 m/s, respectively, which does not drive the observed significant broadening (the ratio of the MDC widths is $\sim$4), and (iii) the angular resolution and other experimental conditions are exactly the same in the LH and LV. Therefore, it is likely that the broadening originates from the differences in the $k_\perp$-broadening effect between the d_{xy}- and the d_{yz}/d_{zx}-derived states. In other words, the spectral behavior probably originates from the presence (absence) of stationary points at the ARPES-measured plane for the d_{xy} (d_{yz}/d_{zx}) states at the (110) surface of SVO, reflecting the presence (absence) of the mirror symmetry in the corresponding states with respect to the ARPES-measured plane.

In order to address the issue in more detail, we have performed ARPES measurements along the *crystallographically equivalent* Γ-M direction at the (001) surface of the SVO film [Fig. 1(b)] under the same experimental conditions except

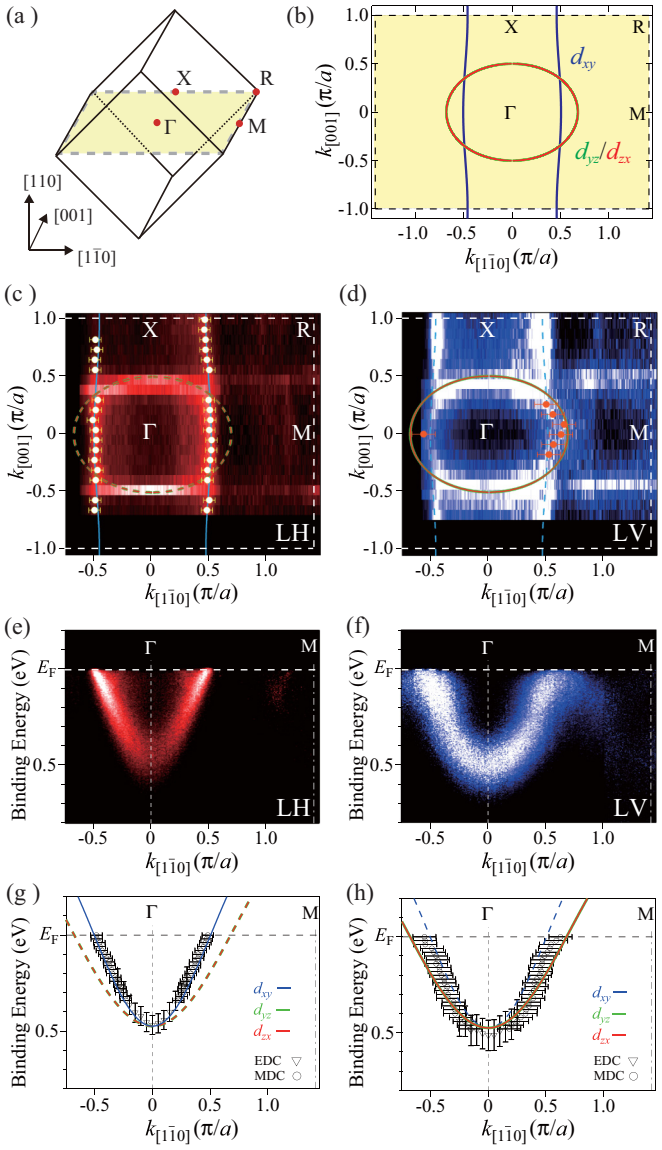

FIG. 3. In-plane FSs and band structures of $SrVO_3$ (110) films. (a) BZ of the SVO (110) surface where the ARPES measurements were performed for the ΓMRX plane (hatched by yellow). (b) FSs calculated from the TB calculation for the ARPES-measured (the ΓMRX) plane. The blue parallel-line FS originates from the d_{xy} states, while the two degenerated ellipses are centered at the Γ point from the d_{yz} and d_{zx} ones. (c), (d) In-plane FS mappings taken at the photon energy of 66 eV that corresponds to the ΓMRX plane using (c) LH and (d) LV light. The d_{xy}- and d_{yz}/d_{zx}-derived FSs obtained from the TB calculation are superimposed as solid blue lines and dotted green/red lines, respectively, for (c) and as dotted blue lines and solid green/red lines, respectively, for (d). The FS determined by ARPES is in good agreement with the result of the TB calculation. (e), (f) ARPES images along the Γ-M high-symmetry line taken at 66 eV with LH and LV light, respectively. Owing to the selection rule for the present experimental setup, the d_{xy} band is dominant in (e), whereas the d_{yz} and d_{zx} bands are dominant in (f). (g), (h) Plots of peak positions determined from the ARPES data in (e) and (f) in comparison with the corresponding results of the TB calculation in the mass renormalization scheme for each 3d t_{2g} orbital. The best fit for the experimental results is obtained with the mass renormalization factor of 0.5.

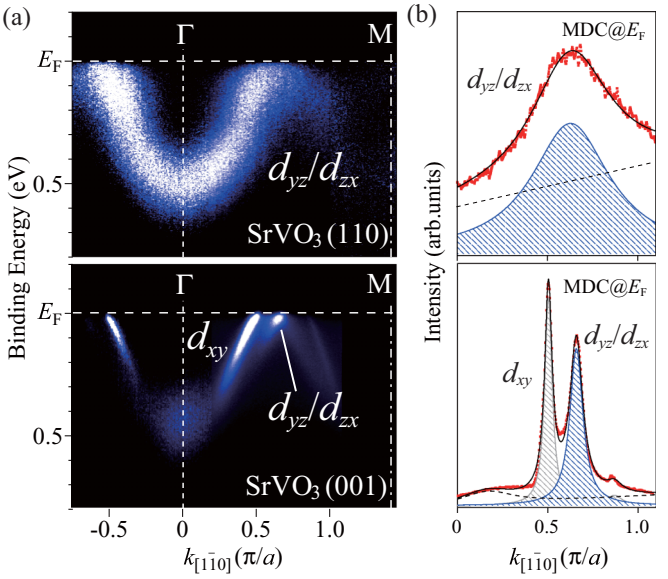

FIG. 4. ARPES images along the Γ-M line of $SrVO_3$ (110) and (001) surfaces. (a) Comparison of ARPES images taken along the crystallographically equivalent Γ-M direction between the SVO (110) surface (upper panel) and the (001) surface (lower panel). The positional relationships between the ARPES-measurement direction and the surface orientation of the SVO film are illustrated in Figs. 1(a) and 1(b). Owing to the selection rule for the present experimental setup, only the d_{yz}/d_{zx} bands are best observed in LV along the Γ-M direction at the (110) surface, whereas both the d_{yz}/d_{zx} bands and the d_{xy} band are observed along the Γ-M direction at the (001) surface. The observed ARPES images for the d_{yz}/d_{zx} bands at the (110) surface are much broader than those at the (001) surface. (b) MDC at E_F along the Γ-M line at the (110) surface (upper panel) and the (001) surface (lower panel). The MDCs have been fitted to a linear combination of a Lorentzian function(s) [a hatched peak(s)] with a smooth background (dashed line).

for the crystal orientation. The results are shown in Fig. 4 in comparison with those along the Γ-M direction at the (110) surface [the same ARPES image data as in Fig. 3(f)]. It should be noted that both the d_{xy}- and d_{yz}/d_{zx}-derived bands are equally observed at the (001) surface in the present experimental geometry. In comparison with the (110) surface, it is evident that the d_{yz}/d_{zx} states in ARPES images taken at the (001) surface are observed as sharp structures and their MDC widths are comparable with those of the d_{xy} states. The slight difference in the MDC width at E_F between d_{yz}/d_{zx} ($0.09\pi/a$) and d_{xy} ($0.06\pi/a$) is well explained by the difference in the Fermi velocities [3.3×10^5 m/s for d_{yz}/d_{zx} and 2.3×10^5 m/s for d_{xy}]. The broadening of the ARPES images at the (110) surface is highlighted at the MDC at E_F as shown in the right panel of Fig. 4. The width of the MDC in the d_{yz}/d_{zx} states observed at the (110) surface is 5.8 times that at the (001) surface. These results strongly suggest that the $k_\perp$ broadening considerably affects the ARPES line shape and the effect strongly depends on the existence of mirror symmetry in the observed states with respect to the ARPES-measured plane, namely, the existence of a stationary point in the vicinity of the ARPES-measurement line (plane). Indeed, the width of the MDC at E_F in the d_{xy} state at the (110) surface, which

has the mirror symmetry with the ARPES-measured plane, is comparable to that at the (001) surface.

B. Simulation of ARPES spectra by treating the $k_\perp$ broadening

In order to analyze the $k_\perp$-broadening effect on ARPES spectra, we have simulated the ARPES spectra as follows. The theoretical ARPES spectrum $D^{\mathrm{ARPES}}(E)$ is described by the one-dimensional DOS along $k_\perp$ weighted by the Lorentzian function representing the $k_\perp$ broadening,

$$D^{\mathrm{ARPES}}(E,k_\parallel) \propto \int_{-\infty}^{\infty} \frac{1}{|\partial E(\boldsymbol{k})/\partial k_\perp|} \frac{\Delta k_\perp}{(k_\perp - k_\perp^0)^2 + (\Delta k_\perp/2)^2} dk_\perp, \tag{1}$$

where $E(\boldsymbol{k})$ is the energy-band dispersion, $k_\parallel$ is the in-plane momentum, $\Delta k_\perp$ is the width of $k_\perp$ broadening, and $k_\perp^0$ is the corresponding measured $k_\perp$ point [3]. In the ARPES measurement, $k_\perp^0$ and $k_\parallel$ are determined as functions of polar angle θ and photon energy $h\nu$,

$$\begin{aligned} k_\parallel &= \sqrt{\frac{2mE_K}{\hbar}} \sin(\theta), \\ k_\perp^0 &= \sqrt{\frac{2m}{\hbar}[E_K \cos^2(\theta) + V_0]}, \\ E_K &= h\nu - E_B - \phi, \end{aligned} \tag{2}$$

where m is the electron mass, $\hbar$ is the reduced Planck constant, E_K is the kinetic energy of the emitted photoelectrons, V_0 is the inner potential, E_B is the binding energy of the electrons in a solid, and ϕ is the work function of a solid [44]. For the simulation, we have employed the results of TB calculations with the renormalization factor of $Z = 0.5$, at which the best fits to the experimental band are obtained as shown in Fig. 3. The value of $\Delta k_\perp$ is estimated to be 0.5 $\mathrm{\AA}^{-1}$ from the equation of Tanuma *et al.* [6]. For simplicity, the value of $k_\perp^0$ is fixed to be 0 so as to trace the ARPES-measurement planes [the ΓMRX plane for the (110) surface and the ΓMX plane for the (001) surface] in the present simulation. The variation of $k_\perp^0$ with changing θ hardly affects the simulation results in the present case as long as the variation is within $\Delta k_\perp$, although the $k_\perp^0$ traces on an elliptical arc obtained from Eq. (2) as a function of $h\nu$ and θ in the ARPES measurement. To mimic the present ARPES images, we calculated the series of ARPES spectra along $k_\parallel$ (the Γ-M direction) using Eq. (1), see the Supplemental Material [38]. First, we defined a rectangle mesh on the ΓMX and ΓMRX emission planes with 141 $k_\parallel$'s and 1001 $k_\perp$'s and calculated the band energy at each $k_\parallel$ point along the $k_\perp$ direction for (110) and (001) surfaces, respectively. Then, we obtained the band dispersions along $k_\perp$ at each $k_\parallel$. We determined the group-velocity v_g by taking the derivative of the band dispersion and calculated the $D^{\mathrm{ARPES}}(E)$ at each $k_\parallel$ by integrating the $1/|v_g|$ weighted by the Lorentzian function along $k_\perp$ using Eq. (1). Thus, we obtained 141 theoretical ARPES spectra for both the (110) and (001) surfaces by convoluting the $D^{\mathrm{ARPES}}(E)$ with a Gaussian with a 30-meV width representative of the experimental energy resolution. Finally, the theoretical-ARPES-derived band structures obtained from the ΓMX and ΓMRX emission planes are mapped out as shown in Figs. 5(a) and 5(b), which correspond to the ARPES images taken along the Γ-M direction at the (110) and (001) surfaces, respectively.

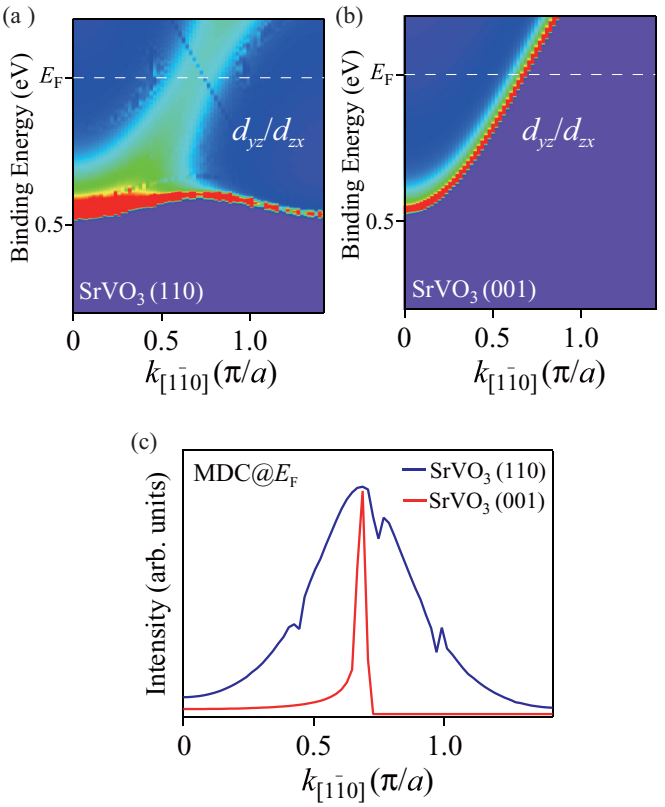

FIG. 5. Simulation results of ARPES spectra along the Γ-M line at (a) the (110) surface and (b) the (001) surface. (c) MDCs at E_F simulated for the (110) and (001) surfaces. The simulation successfully reproduces the key aspects of the ARPES results shown in Fig. 4.

Compared to the theoretical ARPES images in Fig. 5 with the corresponding ARPES images in Fig. 4, the characteristics of the observed ARPES images are well reproduced by the simulation: The ARPES images for the d_{yz}/d_{zx} bands at the (110) surface are significantly broader than those at the (001) surface as a result of $k_\perp$ broadening. In order to discuss the $k_\perp$-broadening effect quantitatively, a comparison of the width of the simulated MDCs at E_F between the (110) and (001) surfaces is shown in Fig. 5(c). The widths of the simulated MDC at E_F are evaluated to be $0.50\pi/a$ and $0.03\pi/a$ for the (110) and (001) surfaces, respectively. The width of simulated MDC at E_F is in excellent agreement with the experimental one ($0.52\ \pi/a$) for the (110) surface, although the simulation result for the (001) surface underestimates the width. This underestimation may originate from the fact that the contributions from the finite angular (momentum) resolution and the impurity scattering in the experiment are not incorporated in the present simulations [45].

The difference in the MDC widths between "the same d_{yz}/d_{zx} bands" is explained as follows. For the (001) surface, the d_{yz}/d_{zx} band should have stationary points along the $k_\perp$ direction at the Γ-M high-symmetry line (also at the whole ARPES-measured ΓMX plane) as a result of the mirror symmetry. Thus, the ARPES spectra mainly reflect the information

on the electronic structures at the high-symmetry line (plane) irrespective of the significant $k_\perp$-broadening effect because the DOS is predominately higher on the high-symmetry lines (planes) owing to the existence of vHS at the whole ARPES-measured ΓMX plane, see the Supplemental Material [38]. In contrast, for the (110) surface, these bands do not have the vHS at the Γ-M high-symmetry line (the ARPES-measured ΓMRX plane), except at the Γ point. Thus, around the Γ point, ARPES spectra mainly reflect the information of the stationary points as long as the trajectory of the stationary points is within the "$k_\perp$-broadening window" of $k_\perp^0 \pm \Delta k_\perp$. However, away from the Γ point, the ARPES spectra are described by the integration of $1/|v_g|$ ($v_g \neq 0$) along $k_\perp$ weighted by the $k_\perp$ broadening [Eq. (1)]. In other words, since the ARPES spectra represent the averaged information within the $k_\perp$-broadening window, the energy distribution curves (EDCs) in the ARPES images are significantly broadened as a result of the $k_\perp$ broadening. The broadening in the EDC (the line shape of the ARPES spectra) causes the simultaneous broadening in the MDC width ($\Delta k_\parallel$) in the ARPES images, see the Supplemental Material [38]. In fact, as the $\Delta k_\perp$ approaches 0 in the simulation, the difference in the MDC peak width between (001) and (110) becomes negligible. In contrast, for the case of the opposite limit ($\Delta k_\perp \to \infty$) [46], $D^{\mathrm{ARPES}}(E)$ reflects the band structure along the high-symmetry lines with mirror symmetry. These results indicate that the consideration of the mirror symmetry of the band structures with respect to the ARPES-measurement plane is important for analyzing the ARPES-spectral line shape in the case that the $k_\perp$-broadening effect is dominant in the ARPES spectra. It should be noted that similar sharp structures are obtained for the d_{xy} states at the (110) surface as in the case of the (001) surface since the d_{xy} band has mirror symmetry with respect to the measurement plane at both surfaces, see the Supplemental Material [38].

The present experimental and simulation results provide important implications for analyzing ARPES spectra of 3D materials. In many cases, the band structures along high-symmetry lines (on the high-symmetry planes) in the BZ are likely to appear as prominent well-resolved structures in the ARPES spectra of 3D materials. Consequently, it is conventionally assumed that the band structure (Fermi surface) along the high-symmetry line (on the high-symmetry plane) is obtained even though the trajectory of the measured $\boldsymbol{k}$ point deviates from the high-symmetry line (plane) [1,2,11]. However, the present studies have demonstrated that this common interpretation of ARPES spectra on 3D materials is valid as long as the electronic structure has mirror symmetry with respect to the ARPES-measured high-symmetry line (plane), namely, the vHS point always exists on the measured high-symmetry line (plane). Furthermore, a stationary point (line) midway between the high-symmetry lines (planes) also appears as a distinct structure in the ARPES spectra since the v_g along the $k_\perp$ direction is also zero on the point (line) [2,7–10], see the Supplemental Material [38]. Thus, for analyzing the ARPES data of 3D materials, it is indispensable to pay special attention to the relationship between the vHS point and the measured $k_\perp$-broadening window of $k_\perp^0 \pm \Delta k_\perp$.

Finally, we briefly discuss the discrepancies between the experimental results and the simulations. As can be seen in Fig. 5, at first glance, the simulation qualitatively describes the different broadening behaviors depending on the crystal surface, especially for the MDC width at E_F. However, a closer look at the result of the (110) surface reveals that there are considerable differences between the experimental and simulation results around the bottom of the conduction band. In the simulation, an almost flat band exists around the binding energy of 0.4–0.5 eV of which the spectral intensity steeply weakens from the Γ to the M point; this is hardly seen in the experiments [see Fig. 4(a)]. The flat band in the simulation originates from the stationary point of the d_{yz}/d_{zx} band running along the [100] and/or [010] direction(s) owing to the long tail of the Lorentzian function representing the $k_\perp$-broadening effects, see the Supplemental Material [38]. Indeed, the flat band disappears at the utmost limit of $\Delta k_\perp = 0$ in the simulations, whereas it becomes a prominent structure in the case of $\Delta k_\perp \to \infty$. The reason why the flat band predicted from the simulation is not observed in the present ARPES experiment is unclear at the moment. The simulation incorporating the lifetime broadening of photoelectrons and/or angular resolution in the apparatus does not explain the absence of the flat band. Meanwhile, a weak but distinct Umklapp band reflecting the surface BZ of the (110) orientation is observed in the ARPES images shown in Fig. 3. These results suggest one possible explanation that certain interference between the surface states and the emitted electrons may affect the ARPES-spectral function [47]. For a quantitative description of the ARPES spectra for 3D materials, a more realistic treatment of the $k_\perp$-broadening effect as well as further investigations of the relationship between the $k_\perp$ broadening and the mirror symmetry (the trajectory of the $v_g = 0$ point) are required. In particular, it is interesting to investigate how the observed $k_\perp$-broadening effect in SVO changes with reducing the film thickness (dimensionality from 3D to 2D), which may provide useful information for settling the controversial interpretation of the 2DEG states at the STO (110) and (111) surfaces [19,20,31].

IV. CONCLUSION

We have performed *in situ* ARPES studies using the variable polarization of synchrotron light for the (110) and (001) surfaces of $SrVO_3$ films in order to examine the effect of $k_\perp$ broadening on ARPES spectra as well as to investigate the electronic structure of $SrVO_3$ films. Using the polarization dependence for the band structures of V 3d t_{2g} states, we have separately observed the d_{xy}- and d_{yz}/d_{zx}-derived states for the (110) surface owing to the dipole selection rule in the present experimental geometry. It is found that the ARPES images for the d_{yz}/d_{zx} states are considerably broader than those for the d_{xy} states at the (110) surface. In contrast, such a broadening is not observed in the d_{yz}/d_{zx}-derived band dispersion along the crystallographically equivalent direction of the (001) surface, indicating that the broadening of the ARPES image originates from the change in the symmetry and the resultant deviation of the trajectory of the stationary points from the high-symmetry line (the ARPES-measured line). The simulation treating the $k_\perp$ broadening in the photoelectron emission process successfully reproduces the key aspect of our ARPES data. These results indicate that the consideration of the mirror symmetry of band structures with respect to

the ARPES-measured plane is important for analyzing the ARPES-spectral line shape in the case that the $k_\perp$-broadening effect is dominant in the ARPES spectra.

ACKNOWLEDGMENTS

The authors are very grateful to S. Ishibashi for the useful discussions. This work was supported by a Grant-in-Aid for Scientific Research (Grants No. B25287095, No. 15H02109, and No. 16H02115) and a Grant-in-Aid for Young Scientists (Grants No. 26870843 and No. 15K17470) from the Japan Society for the Promotion of Science (JSPS) and the MEXT Element Strategy Initiative to Form Core Research Center. M.K. acknowledges financial support from JSPS for Young Scientists. The work at KEK-PF was performed under the approval of the Program Advisory Committee (Proposals No. 2016T001, No. 2013S2-002, No. 2014G678, and No. 2015S2-005) at the Institute of Materials Structure Science, KEK.

[1] T. Grandke, L. Ley, and M. Cardona, Phys. Rev. B **18**, 3847 (1978).
[2] H. Kumigashira, H.-D. Kim, T. Ito, A. Ashihara, T. Takahashi, T. Suzuki, M. Nishimura, O. Sakai, Y. Kaneta, and H. Harima, Phys. Rev. B **58**, 7675 (1998).
[3] V. N. Strocov, J. Electron Spectrosc. Relat. Phenom. **130**, 65 (2003).
[4] S. Hüfner, *Photoelectron Spectroscopy*, 3rd ed. (Springer-Verlag, Berlin, 2003).
[5] C. J. Powell and A. Jablonski, Nucl. Instrum. Methods Phys. Res. Sect. A **601**, 54 (2009).
[6] S. Tanuma, C. J. Powell, and D. R. Penn, Surf. Interf. Anal. **43**, 689 (2011).
[7] H. Kumigashira, H.-D. Kim, A. Ashihara, A. Chainani, T. Yokoya, T. Takahashi, A. Uesawa, and T. Suzuki, Phys. Rev. B **56**, 13654 (1997).
[8] H. Kumigashira, T. Ito, A. Ashihara, H.-D. Kim, H. Aoki, T. Suzuki, H. Yamagami, T. Takahashi, and A. Ochiai, Phys. Rev. B **61**, 15707 (2000).
[9] T. Ito, H. Im, S.-I. Kimura, and Y.-S. Kwon, J. Magn. Magn. Mater. **310**, 431 (2007).
[10] J. Krempaský, V. N. Strocov, P. Blaha, L. Patthey, M. Radović, M. Falub, M. Shi, and K. Hricovini, J. Electron Spectrosc. Relat. Phenom. **181**, 63 (2010).
[11] H. Wadati, T. Yoshida, A. Chikamatsu, H. Kumigashira, M. Oshima, H. Eisaki, Z.-X. Shen, T. Mizokawa, and A. Fujimori, Phase Transitions **79**, 617 (2006).
[12] S.-I. Fujimori, T. Ohkochi, T. Okane, Y. Saitoh, A. Fujimori, H. Yamagami, Y. Haga, E. Yamamoto, and Y. Ōnuki, Phys. Rev. B **86**, 235108 (2012).
[13] I. H. Inoue, O. Goto, H. Makino, N. E. Hussey, and M. Ishikawa, Phys. Rev. B **58**, 4372 (1998).
[14] E. Pavarini, A. Yamasaki, J. Nuss, and O. K. Andersen, New J. Phys. **7**, 188 (2005).
[15] M. Takizawa, M. Minohara, H. Kumigashira, D. Toyota, M. Oshima, H. Wadati, T. Yoshida, A. Fujimori, M. Lippmaa, M. Kawasaki, H. Koinuma, G. Sordi, and M. Rozenberg, Phys. Rev. B **80**, 235104 (2009).
[16] K. Yoshimatsu, K. Horiba, H. Kumigashira, T. Yoshida, A. Fujimori, and M. Oshima, Science **333**, 319 (2011).
[17] M. Kobayashi, K. Yoshimatsu, E. Sakai, M. Kitamura, K. Horiba, A. Fujimori, and H. Kumigashira, Phys. Rev. Lett. **115**, 076801 (2015).
[18] T. Yoshida, M. Kobayashi, K. Yoshimatsu, H. Kumigashira, and A. Fujimori, J. Electron Spectrosc. Relat. Phenom. **208**, 11 (2016).
[19] Z. Wang, Z. Zhong, X. Hao, S. Gerhold, B. Stöger, M. Schmid, J. Sánchez-Barriga, A. Varykhalov, C. Franchini, K. Held, and U. Diebold, Proc. Natl. Acad. Sci. U.S.A. **111**, 3933 (2014).
[20] T. C. Rödel, C. Bareille, F. Fortuna, C. Baumier, F. Bertran, P. Le Fèvre, M. Gabay, O. Hijano Cubelos, M. J. Rozenberg, T. Maroutian, P. Lecoeur, and A. F. Santander-Syro, Phys. Rev. Appl. **1**, 051002 (2014).
[21] W. Meevasana, X. J. Zhou, B. Moritz, C.-C. Chen, R. H. He, S.-I. Fujimori, D. H. Lu, S.-K. Mo, R. G. Moore, F. Baumberger, T. P. Devereaux, D. van der Marel, N. Nagaosa, J. Zaanen, and Z.-X. Shen, New J. Phys. **12**, 023004 (2010).
[22] A. F. Santander-Syro, O. Copie, T. Kondo, F. Fortuna, S. Pailhès, R. Weht, X. G. Qiu, F. Bertran, A. Nicolaou, A. Taleb-Ibrahimi, P. Le Fèvre, G. Herranz, M. Bibes, N. Reyren, Y. Apertet, P. Lecoeur, A. Barthélémy, and M. J. Rozenberg, Nature (London) **469**, 189 (2011).
[23] W. Meevasana, P. D. K. King, R. H. He, S.-K. Mo, M. Hashimato, A. Tamai, P. Songsiriritthigul, F. Baumberger, and Z.-X. Shen, Nat. Mater. **10**, 114 (2011).
[24] R. Yukawa, S. Yamamoto, K. Ozawa, M. D'Angelo, M. Ogawa, M. G. Silly, F. Sirotti, and I. Matsuda, Phys. Rev. B **87**, 115314 (2013).
[25] A. F. Santander-Syro, F. Fortuna, C. Bareille, T. C. Rödel, G. Landolt, N. C. Plumb, J. H. Dil, and M. Radović, Nat. Mater. **13**, 1085 (2014).
[26] P. D. C. King, S. McKeown Walker, A. Tamai, A. de la Torre, T. Eknapakul, P. Buaphet, S.-K. Mo, W. Meevasana, M. S. Bahramy, and F. Baumberger, Nat. Commun. **5**, 3414 (2014).
[27] N. C. Plumb, M. Salluzzo, E. Razzoli, M. Månsson, M. Falub, J. Krempasky, C. E. Matt, J. Chang, M. Schulte, J. Braun, H. Ebert, J. Minár, B. Delley, K.-J. Zhou, T. Schmitt, M. Shi, J. Mesot, L. Patthey, and M. Radović, Phys. Rev. Lett. **113**, 086801 (2014).
[28] S. McKeown Walker, F. Y. Bruno, Z. Wang, A. de la Torre, S. Riccó, A. Tamai, T. K. Kim, M. Hoesch, M. Shi, M. S. Bahramy, P. D. C. King, and F. Baumberger, Adv. Mater. **27**, 3894 (2015).
[29] C. Chen, J. Avila, E. Frantzeskakis, A. Levy, and M. C. Asensio, Nat. Commun. **6**, 8585 (2015).
[30] Z. Wang, S. McKeown Walker, A. Tamai, Y. Wang, Z. Ristic, F. Y. Bruno, A. de la Torre, S. Riccò, N. C. Plumb, M. Shi, P. Hlawenka, J. Sánchez-Barriga, A. Varykhalov, T. K. Kim, M. Hoesch, P. D. C. King, W. Meevasana, U. Diebold, J. Mesot, B. Moritz, T. P. Devereaux, M. Radovic, and F. Baumberger, Nature Mater. **15**, 835 (2016).
[31] S. McKeown Walker, A. de la Torre, F. Y. Bruno, A. Tamai, T. K. Kim, M. Hoesch, M. Shi, M. S. Bahramy, P. D. C. King, and F. Baumberger, Phys. Rev. Lett. **113**, 177601 (2014).

[32] P. D. C. King, R. H. He, T. Eknapakul, P. Buaphet, S.-K. Mo, Y. Kaneko, S. Harashima, Y. Hikita, M. S. Bahramy, C. Bell, Z. Hussain, Y. Tokura, Z.-X. Shen, H. Y. Hwang, F. Baumberger, and W. Meevasana, Phys. Rev. Lett. **108**, 117602 (2012).

[33] A. F. Santander-Syro, C. Bareille, F. Fortuna, O. Copie, M. Gabay, F. Bertran, A. Taleb-Ibrahimi, P. Le Fèvre, G. Herranz, N. Reyren, M. Bibes, A. Barthélémy, P. Lecoeur, J. Guevara, and M. J. Rozenberg, Phys. Rev. B **86**, 121107(R) (2012).

[34] C. Bareille, F. Fortuna, T. C. Rödel, F. Bertran, M. Gabay, O. Hijano Cubelos, A. Taleb-Ibrahimi, P. Le Fèvre, M. Bibes, A. Barthélémy, T. Maroutian, P. Lecoeur, M. J. Rozenberg, and A. F. Santander-Syro, Sci. Rep. **4**, 3586 (2014).

[35] G. Berner, M. Sing, H. Fujiwara, A. Yasui, Y. Saitoh, A. Yamasaki, Y. Nishitani, A. Sekiyama, N. Pavlenko, T. Kopp, C. Richter, J. Mannhart, S. Suga, and R. Claessen, Phys. Rev. Lett. **110**, 247601 (2013).

[36] C. Cancellieri, M. L. Reinle-Schmitt, M. Kobayashi, V. N. Strocov, P. R. Willmott, D. Fontaine, Ph. Ghosez, A. Filippetti, P. Delugas, and V. Fiorentini, Phys. Rev. B **89**, 121412(R) (2014).

[37] K. Horiba, H. Ohguchi, H. Kumigashira, M. Oshima, K. Ono, N. Nakagawa, M. Lippmaa, M. Kawasaki, and H. Koinuma, Rev. Sci. Instrum. **74**, 3406 (2003).

[38] See Supplemental Material at http://link.aps.org/supplemental/10.1103/PhysRevB.94.125148 for more details of experimental geometry, out-of-plane FS mappings, and simulation results for ARPES spectra.

[39] A. Damascelli, Z. Hussain, and Z.-X. Shen, Rev. Mod. Phys. **75**, 473 (2003).

[40] Ph. Hofmann, Ch. Søndergaard, S. Agergaard, S. V. Hoffmann, J. E. Gayone, G. Zampieri, S. Lizzit, and A. Baraldi, Phys. Rev. B **66**, 245422 (2002).

[41] C. Liu, T. Kondo, N. Ni, A. D. Palczewski, A. Bostwick, G. D. Samolyuk, R. Khasanov, M. Shi, E. Rotenberg, S. L. Bud'ko, P. C. Canfield, and A. Kaminski, Phys. Rev. Lett. **102**, 167004 (2009).

[42] R. S. Dhaka, T. Das, N. C. Plumb, Z. Ristic, W. Kong, C. E. Matt, N. Xu, K. Dolui, E. Razzoli, M. Medarde, L. Patthey, M. Shi, M. Radović, and J. Mesot, Phys. Rev. B **92**, 035127 (2015).

[43] K. Horiba, M. Kitamura, K. Yoshimatsu, M. Minohara, E. Sakai, M. Kobayashi, A. Fujimori, and H. Kumigashira, Phys. Rev. Lett. **116**, 076401 (2016).

[44] F. J. Himpsel, Adv. Phys. **32**, 1 (1983).

[45] The contribution of these effects to additional broadening in the width of the MDC at E_F is roughly estimated to be 0.08–0.09π/a. The additional broadening hardly affects the MDC width for the (110) surface.

[46] P. J. Feibelman and D. E. Eastman, Phys. Rev. B **10**, 4932 (1974).

[47] S. W. Jung, W. J. Shin, J. Kim, L. Moreschini, H. W. Yeom, E. Rotenberg, A. Bostwick, and K. S. Kim, Phys. Rev. Lett. **116**, 186802 (2016).